Small flank failure of Anak Krakatau Volcano caused catastrophic December 2018 Indonesian tsunami

Authors: Rebecca Williams[1*], Pete Rowley[1], Matthew C. Garthwaite[2]

[1]Department of Geography, Geology & Environment, University of Hull, Hull, UK.

[2]Positioning and Community Safety Division, Geoscience Australia, Canberra, ACT, Australia.

*Correspondence to: Rebecca.williams@hull.ac.uk.

Volcanogenic tsunamis are one of the deadliest volcanic phenomena[1]. Understanding their triggering processes and mitigating their effect remains a major challenge. On 22 December 2018, flank failure of the Anak Krakatau volcano, Indonesia generated a tsunami which killed 431 people[2]. This event was captured in unprecedented detail by high-resolution satellite imagery and eyewitness accounts[3–6]. Here we combine historic observations[7–9] with these recent data to - for the first time - interpret the internal architecture of Anak Krakatau, and reconstruct the failure, tsunamigenesis and regrowth processes observed. We calculate the volume of material initially lost from the volcano flank failure and find that it was relatively small (~0.1 km^3) compared to the overall changes observed during the entire eruption, but was nonetheless able to generate rapid tsunami waves with devastating impacts. The flank failure also changed the eruption style and upper volcanic plumbing system, with these subsequent explosive eruptions destroying the summit and then partially rebuilding the lost flank. The nature of the flank failure was controlled by the internal structure of the island, and - although regrowth rate will be a

primary control on flank failure intervals - the reconfiguring of the volcano's internal vent network is likely to have re-stabilised it in the medium term. The findings demonstrate that hazard assessments at ocean islands must consider that even small flank failures, during unexceptional eruptions, can have catastrophic consequences.

Volcanogenic tsunamis have caused the deaths of over 55,000 people since 1600 AD [10]. The last three centuries have seen around 100 notable volcanogenic tsunamis produced in the world's oceans [11]. Volcanogenic tsunamis are triggered by a variety of processes, including submarine volcanic explosions, entry of volcanic flows into the ocean, sudden flank deformations, or flank failures, and are not necessarily triggered by a volcanic eruption. Their unpredictability and the high amplitude of generated waves makes volcanogenic tsunamis a significant local and regional hazard, often with catastrophic consequences [11]. However, they occur rarely and there have been very few volcanogenic tsunamis observed in sufficient detail to enable evaluation of their triggering, propagation mechanisms and their impacts (some examples are Stromboli in 2002 [12,13], and Soufrière Hills in 2003[14]).

On 22 December 2018, Anak Krakatau ('Child of Krakatau'), an active volcanic island situated within the Krakatau caldera in the Sunda Strait between Java and Sumatra, Indonesia, experienced a flank failure. This flank failure generated a volcanogenic tsunami, causing widespread damage to the surrounding coastlines (Fig. S1) and was captured in unprecedented detail by remote sensing satellites. Combining these observations with bathymetric and topographic surveys made since the catastrophic 1883 eruption of the Krakatau caldera[7–9], and a recently compiled digital elevation model (DEM)[15], we are able to: (i) reconstruct the internal

architecture of Anak Krakatau prior to the tsunami-generating flank failure; (ii) calculate the volume of collapsed material; and (iii) build a conceptual model for the failure and subsequent regrowth process to mid-January 2019. This work enables new understanding of volcanic flank failures and advances the science of tsunami risk mitigation.

Prior to December 2018, the active volcanic cone of Anak Krakatau had grown to ~300 m above sea level, having first risen above sea-level in 1929[16]. The caldera-forming eruption of Krakatau in 1883 caused the deaths of 36,000 people[10] after pyroclastic density currents entered the ocean and generated a catastrophic tsunami that swept the coasts of the Sunda Strait[17]. Anak Krakatau has frequently erupted since 1927, with eruptions typically strombolian to vulcanian in style, characterized by small explosive eruptions with columns reaching to 2 km in height[8,18,19]. Anak Krakatau is located on the edge of the steep NE wall of the 1883 Krakatau caldera, and its rapid growth, comprising largely of loose pyroclastic material (Fig. 1A), meant that Anak Krakatau was already recognized as an unstable edifice and tsunami risk[9]. Prior to the flank failure, the volcano had been in an active phase since June 2018, producing strombolian eruptions.

At 21:27 Western Indonesian Time (WIB) on 22 December 2018 a tsunami impacted the coasts of the Pandeglang, Serang and South Lampung regions in Indonesia (Fig. S1). The waves ranged in height from 0.27 to 1.40 m (Fig. S1), caused the deaths of 431 people, injured a further 7,200 people, and displaced 46,646 people. There has been significant damage to coastal infrastructure, including 1,778 houses, 78 damaged lodging and warung (small family owned business) units, 434 damaged boats and ships and some damage to public facilities (Press release dated 29 December 2018 15:17 UTC[4]).

On the day of the tsunami, the Anak Krakatau volcano was in an elevated but unexceptional phase of activity[3], undergoing a strombolian-style eruption. An ash column of up to 1.5 km was observed, and earthquake tremors of typical amplitude were recorded (Press release dated 23 December 2018[5,6]. A low frequency 5.1 Mw earthquake, with a NW-SE trending focal plane was recorded at 20:55 WIB on the regional seismic network[20]. Further earthquake activity was recorded at 21.03 WIB and appears to have destroyed the seismometer situated on Anak Krakatau (Press release dated 23 December 2018 00:01 UTC[4]). Twenty-four minutes later, the first tsunami waves reached the surrounding coasts.

The first observation of Anak Krakatau following the flank failure was made by the Sentinel-1A Synthetic Aperture Radar (SAR) satellite, which imaged the volcano at 05:33 WIB on 23 December 2018 (22:33, 22 December 2018 UTC), only ~8 hours after the tsunami impacted the coast. Analysis of this SAR image clearly shows that the western portion of Anak Krakatau had failed and collapsed (Fig. 1C). Subsequent images reveal significant morphological changes to the volcano as the eruption progressed (Fig. 1D-F). Here we interpret the time series of Sentinel-1 SAR images captured from three viewing geometries to understand the mechanisms of the flank failure and tsunami generation and how the volcano responded during the subsequent eruptions.

Our interpretation of the 22 December 2018 (UTC) SAR image reveals a 900 m NNE-SSW trending linear plane along which the western flank has failed (Fig. 2, failure plane A). In addition, a new break in slope has appeared east of this failure, and the block between the failure

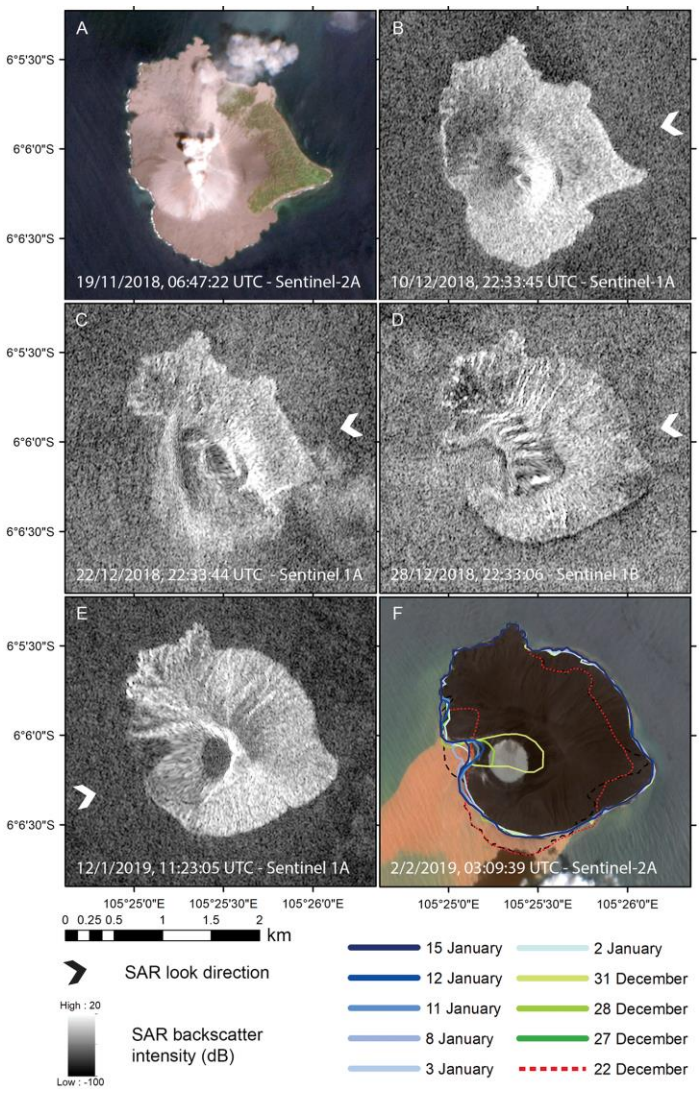

Fig. 1. Satellite imagery showing the evolving geomorphology of Anak Krakatau as a result of the December – January eruptive activity and the 22 December 2018 tsunami. Panel A and B show the island morphology before the flank failure. Panel C was captured only 8 hours after the tsunami and shows the western flank failure and collapse of the summit. Panel D shows the destruction of the summit and Panel E shows the subsequent regrowth of the island. Panel F tracks the changes in island surface area through this period. Panel A and F are Sentinel-2A true colour images and panels B-E are Sentinel-1A and -1B SAR backscatter images. Arrows show the radar looking direction.

and the summit cone exhibits increased reflectance relative to the previously captured radar image (10 December 2018 UTC). Radar backscatter intensity depends on three factors: surface geometry with respect to the incident radar; surface roughness at the scale of the radar wavelength (5.6 cm for Sentinel-1); and the dielectric properties of the surface material[21]. Thus, the increased reflectance could be caused by the deposition of fresh pyroclastic material or disturbed ground. However, the feature is linear, with a sharp transition, so unlikely to be new pyroclastic material. Furthermore, erupted material would be expected to be more radially distributed around the vent. Therefore our interpretation is that the block has coherently rotated with partial slip along this second inland failure plane (Fig. 2, failure plane B. The head of the failing slope has rotated back toward the radar source such that it backscatters more energy, thus also explaining both the new break in slope and the higher radar reflectance. This block appears to have gone by the 28th December (Fig 1D). Collapse of the summit appears to follow the underlying structure of a pre-existing crater on which the modern summit was built[7,8]. The north and eastern flanks of the volcano are largely unaffected by the failure, aside from some minor remodelling of the coastline as a result of the tsunami.

Cross-sections through the edifice illuminate the nature of the failure and help constrain the total volume of lost material during this event (Fig. 3). These show that the island has grown over a basement structure formed during the collapse of the Krakatau caldera in 1883[8]. The core of the Anak Krakatau edifice has migrated westward through time[8,9], which has resulted in the bulk of the modern edifice being built on an array of strata which dip toward the center of the 1883 caldera. This gives a preferential failure direction to the west which may explain the marine inundations of the core of the island from the west (e.g. Fig. 1d-f, and [7]). In our subsequent

analysis only failure plane A is considered as a result of the undefined scale of block rotation failure on plane B.

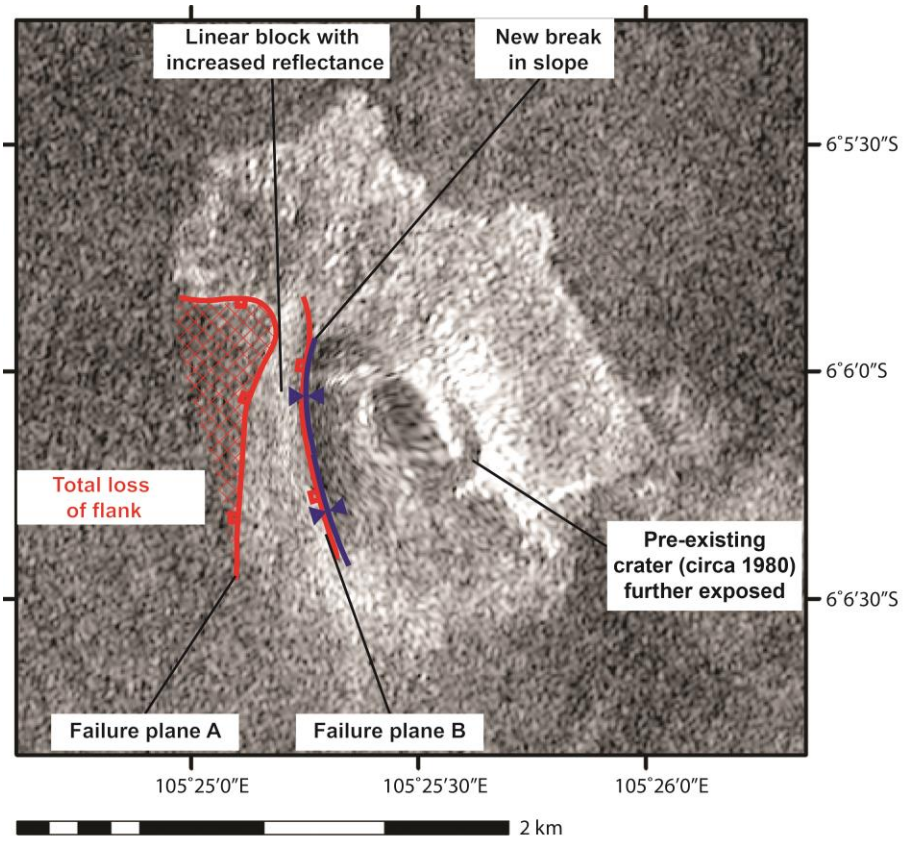

Fig. 2. Interpretation of 22 December 2018 Sentinel-1A SAR image, showing two discrete failure planes; plane A which has enabled complete loss of its hanging wall material, and plane B which has resulted in a rotational slide of the linear block between the failure planes, with an undefined magnitude of slip.

Subaerial failure volume is calculated using the failure area observed in the 22 December 2018 SAR image and volumetrically constrained by the DEM. Submarine failure is calculated by cross-section analysis of the island (Fig. 3) assuming a simple listric detachment of failure plane A. We calculate volumes of 0.004 km^3 for the subaerial failure, and in the order of 0.1 km^3 for

the submarine failure. This places the subaerial volume within the error of the submarine volume. This is small for a volcanic flank failure; terrestrial flank failures at volcanoes have had volumes up to 10 km^3, and submarine volcanic flank failures up to 5000 km^3 are known to have occurred[22–25].

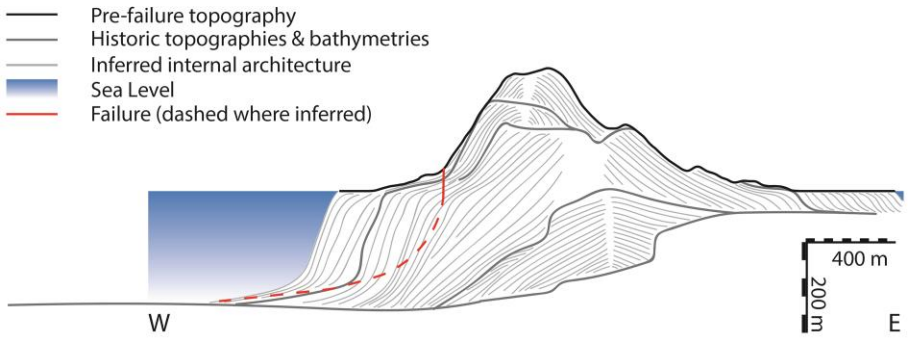

Fig. 3. A west-east cross section through Anak Krakatau (2x vertical exaggeration) showing the subaerial failure plane A (solid red line) and the inferred submarine failure plane (dashed red line).

The flank failure was followed by a significant change in subsequent eruptive activity (Fig. 4) and migration of the eruption vent multiple times between 22 December 2018 and 12 January 2019. Following the failure, aerial photography taken on 23 December 2018 (Fig. S2) shows an eruptive column centered offshore of the failure scarp. We propose that the flank failure decompressed the plumbing system sufficiently that a new magma pathway was opened, which resulted in a new submarine vent ~500 m west of the pre-existing vent. This allowed the incursion of water into the vent, producing the violent phreatomagmatic eruptions observed on 23 December 2018. It is this explosive activity that removed the remaining portion of the western flank and the summit of the volcano. Over the following three weeks, as new pyroclastic material

and collapse material was added to the failed submarine structure, the vent migrated back toward its original location (Fig.1 d-f, Fig. S2, Movies S1-S3). As new eruptive material was added, and the submarine flanks experienced smaller mass movements to recover a stable angle of repose, the stress regime on the plumbing system returned toward its earlier state, resulting in reactivation of the pre-failure magma pathway (Fig. 4).

Flank failure and the generation of a tsunami was a known hazard for Anak Krakatau. Giachetti et al.[9] modelled a failure of 0.28 km^3 of the western flank, estimating wave heights on the coastlines of the Sunda Strait ranging from 0.3 m to 3.4 m. Our estimate of the 2018 flank failure is much smaller in volume (3x smaller; ~0.1 km^3). However, for three locations, the waves were as high as those modelled by Giachetti et al. The waves arrived on the coasts of Java and Sumatra within 24-37 minutes, 10 minutes quicker than modelled for Java and over 20 minutes quicker than modelled for Sumatra[9]. Hence, the speed of the tsunami waves were substantially underestimated in the model and future tsunami hazard assessments for the Sunda Strait must consider these more rapid wave velocities.

We show that the flank failure was unexceptional, meaning that an extraordinary event was not required to trigger the tsunami, yet it had catastrophic consequences. The flank failure occurred during a normal eruptive episode, likely due to over steepening of the western flank on the edge of the 1883 caldera combined with alteration-related weakening of the deeper Anak-Krakatau stratigraphy. The volume of the flank failure was small, compared to predicted failure volumes and flank failures at other volcanoes, yet it generated a tsunami as large as and faster than modelled with a significantly larger failure. Significant regrowth of the island will be needed

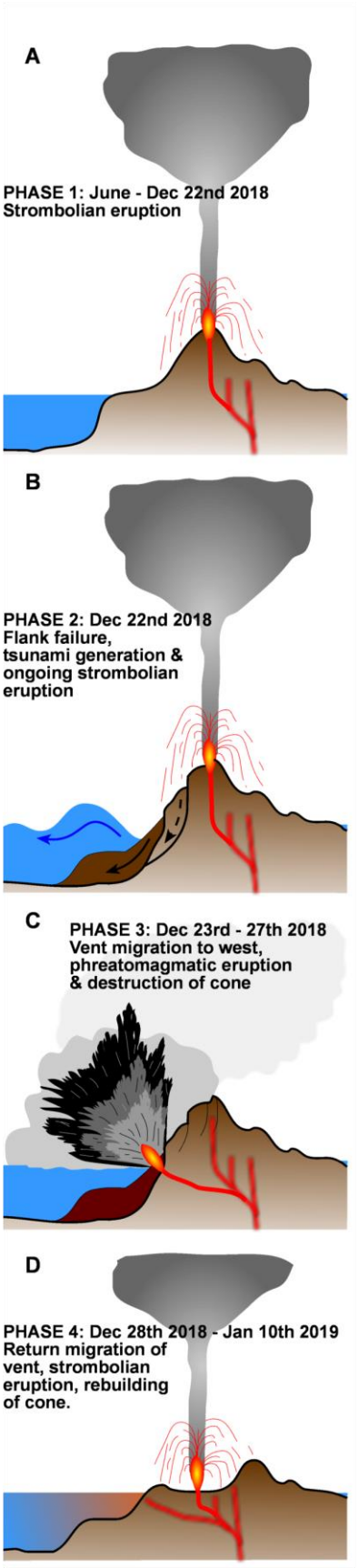

before flank failure is likely to occur again, but the underlying submarine architecture has been extensively remodelled. As a result, the failure criteria will be different for subsequent flank failures. Therefore, establishing the new bathymetry and submarine stratigraphy following the 2018 flank failure is critical to strengthen the reliability of any future failure assessments of the volcano, and in understanding the hazard at other island volcanoes. Finally, this study also highlights that existing hazard assessments at volcanic islands are very likely underestimating the risks from volcanogenic tsunamis due to small (<0.25 km^3) failures.

Fig. 4. Time line of eruptive activity and tsunami generation at Anak Krakatau. Splayed magmatic plumbing in panel A represents an assumed migration of the vent prior to 2018 as interpreted from Fig. 3.

Methods

Synthetic Aperture Radar Processing

We obtained Sentinel-1 "Interferometric Wide Swath" (IWS) SAR products from the Copernicus Open Access Hub in three viewing geometries: two descending orbits and one ascending orbit (Table S1). Each SLC-format SAR product was converted to a "Sigma-0" backscatter coefficient image in slant-range geometry by applying the calibration and noise data annotated in the product metadata. We multi-looked (subsampled) the images to obtain approximately square pixels in radar geometry (4 range looks and 1 azimuth look).

A "master" image captured prior to the 22 December 2018 event was chosen for each of the three viewing geometries. Every other image within the three viewing geometry stacks (i.e. those not chosen as a "master") was then co-registered to its respective "master" image. Co-registration is the process of image alignment that involves measuring range and azimuth offsets between the two images via cross-correlation across a grid of sample windows covering the full image extents. A first-order polynomial transformation function is fitted (constant offset in range and azimuth directions) to the determined offsets and the image resampled to the radar-geometry of the "master" using a 2D Lanczos interpolation (of order 4). Every image was co-registered using an iterative procedure until the azimuth co-registration was better than 1/100 of a pixel. This high accuracy is particularly important if the Sentinel-1 IWS products are to be used for interferometry (not in this case). The result of this step is a stack of aligned radar-geometry images for each viewing geometry (Movie 1).

In a final step, the "master" image was used to derive a geocoding look-up table that can be used to transform the radar-geometry images to map view. This was done by first generating a

simulated radar backscatter image from the 1-arc-second (~30 m) SRTM Digital Elevation Model (DEM) covering the geographic extent of the radar image footprints. This simulated radar image was then transformed to radar geometry using the orbit information annotated in the "master" image's product metadata. Subsequent co-registration between this image and the "master" image was performed to enable a refinement of the transformation parameters to be undertaken. Sentinel-1 image products usually only need a first-order polynomial transformation owing to the high quality of the provided orbit information. The Sentinel-1 image products we have used cover a much larger area than just the Krakatau caldera and include large portions of Java and/or Sumatra. Therefore the accuracy of the co-registration of the "master" images to the simulated radar image is not affected by the highly localised changes occurring at Anak Krakatau between image captures. A refined geocoding look-up table was then derived that provides a transformation to map view for every pixel in the radar-geometry image.

Finally, all radar-geometry images in each viewing geometry were orthorectified using the look-up table. A B-spline interpolation (of order 5) was used to perform the resampling.

Sentinel 2 Data

We obtained Sentinel 2A true colour images (TCI) collected on the 16th November 2018 from the Copernicus Open Access Hub.

Cross-Sections

Bathymetric and topographic surveys from 1918, 1928, 1960 and 1990 are compiled in Figure 3, together with qualitative descriptions of the growth of the edifice, and a recent profile derived from the DEM of the volcano[7–9].

Volume calculations

We obtained a 0.27-arc-second resolution DEM from the Indonesian Geospatial Agency (Badan Informasi Geospasial). This DEM, covering the whole of Indonesia, was constructed from data from TerraSAR-X (from 2011 - 2013), InSAR (from 2000, 2004, 2008, and 2011) and ALOS-PALSAR (2007/2008) (pers. comm. Susilo Sarimun, Badan Informasi Geospasial, 7th February 2019). The heights given in the DEM are therefore relevant to an epoch sometime between 2000 and 2013. The DEM was converted to a triangulated irregular network (TIN), after resampling to a higher resolution grid.

The failure surface area (and outlines of the evolving island shape) was delineated using a combination of Sentinel-2 visible spectrum imagery and SAR data layers. We used aerial photography (Fig. S2) to confirm the failure plane. To calculate the volume of material mobilised in the flank failure, we performed a surface volume calculation on the TIN using ArcGIS 3D Analyst.

We assumed a subvertical failure plane, which is supported by observations made from aerial photography (Fig. S2). Although we have interpreted slip on a second inland plane (Fig. 2), we have not included this in volume calculations since it is impossible to constrain the dip of the plane, or the magnitude of slip. Submarine failure was calculated using analysis of the cross-section (Fig. 3), in which the submarine flank is projected based on the modern extent of the island (as captured in the DEM data), and using the submarine slope recorded in the 1990 bathymetric survey[8]. The failure plane is traced as a standard listric surface, and follows parts of the inferred and observed underlying stratigraphy. The cross-sectional area is multiplied by the failure length (900 m) observed in the SAR imagery (Fig. 1c). The differences in precision used

for the volumes are derived from the resolution of the datasets and calculation methods used for each volume.

Data availability

The Sentinel datasets analysed during the current study are available in the Copernicus Open Access Hub, https://scihub.copernicus.eu/. The DEM analysed is available from the Indonesian Geospatial Agency (Badan Informasi Geospasial) (http://tides.big.go.id/DEMNAS/#Info). Processed datasets generated during the current study are available from the corresponding author on reasonable request.

References:

1. Auker, M. R., Sparks, R. S. J., Siebert, L., Crosweller, H. S. & Ewert, J. A statistical analysis of the global historical volcanic fatalities record. *J. Appl. Volcanol.* **2**, 2–24 (2013).

2. Ramadhan, P. B. Update Terkini Penanganan Bencana Tsunami Selat Sunda, Total 426 Orang Meninggal Dunia. *TRIBUNnews* (2018).

3. Andersen, Ø. L. Krakatau volcano: Witnessing the eruption, tsunami and the aftermath 22-23th December 2018.

4. BNPB. Badan Nasional Penanggulangan Bencana Facebook. Available at: https://www.facebook.com/HumasBNPB/. (Accessed: 22nd January 2019)

5. MAGMA. Multiplatform Application for Geohazard Mitigation and Assessment in Indonesia. Available at: https://magma.vsi.esdm.go.id/. (Accessed: 14th February 2019)

6. PVMBG. Kementerian Energi dan Sumber Daya Mineral Badan Geologi. Available at: http://www.vsi.esdm.go.id/. (Accessed: 22nd January 2019)

7. Decker, R. & Hadikusumo, D. Results of the 1960 expedition to Krakatau. *J. Geophys. Res.* **55**, 3497–3511 (1961).

8. Deplus, C. *et al.* Inner structure of the Krakatau volcanic complex (Indonesia) from gravity and bathymetry data. *J. Volcanol. Geotherm. Res.* **64**, 23–52 (1995).

9. Giachetti, T., Paris, R., Kelfoun, K. & Ontowirjo, B. Tsunami hazard related to a flank collapse of Anak Krakatau Volcano, Sunda Strait, Indonesia. *Geol. Soc. London, Spec. Publ.* **361**, 79–90 (2012).

10. Auker, M. R., Sparks, R. S. J., Siebert, L., Crosweller, H. S. & Ewert, J. A statistical analysis of the global historical volcanic fatalities record. *J. Appl. Volcanol.* **2**, 2–24 (2013).

11. Day, S. J. Chapter 58 - Volcanic Tsunamis. in *The Encyclopedia of Volcanoes (Second Edition)* (ed. Sigurdsson, H.) 993–1009 (Academic Press, 2015). doi:https://doi.org/10.1016/B978-0-12-385938-9.00058-4

12. Bonaccorso, A., Calvari, S., Garfi, G., Lodato, L. & Patanè, D. Dynamics of the December 2002 flank failure and tsunami at Stromboli volcano inferred by volcanological and geophysical observations. *Geophys. Res. Lett.* **30**, (2003).

13. La Rocca, M. *et al.* Seismic signals asssociated with landslides and with a tsunami at Stromboli volcano, Italy. *Bull. Seismol. Soc. Am.* **94**, 1850–1867 (2004).

14. Pelinovsky, E. N. *et al.* Tsunami generated by the volcano eruption on July 12-13, 2003 at Montserrat, Lesser Antilles. *Science of Tsunami Hazards* **22**, 44 (2004).

15. BIG. Seamless Digital Elevation Model (DEM) dan Batimetri Nasional. Available at: http://tides.big.go.id/DEMNAS/#Info. (Accessed: 5th January 2019)

16. Neumann van Padang, M. De Krakatau voorheen en Thans. *Trop. Nat.* **22**, 137–150 (1933).

17. Self, S. & Rampino, M. R. The 1883 eruption of Krakatau. *Nature* **294**, 699–704 (1981).

18. Camus, G., Gourgaud, A. & Vincent, P. M. Petrologic evolution of Krakatau (Indonesia): Implications for a future activity. *J. Volcanol. Geotherm. Res.* **33**, 299–316 (1987).

19. Agustan, Kimata, F., Pamitro, Y. E. & Abidin, H. Z. Understanding the 2007-2008 eruption of Anak Krakatau volcano by combining remote sensing technique and seismic data. *Int. J. Appl. Earth Obs. Geoinf.* **14**, 73–82 (2012).

20. GEOFON Program. Available at: https://geofon.gfz-potsdam.de/eqinfo/event.php?id=gfz2018yzre. (Accessed: 6th February 2019)

21. Di Traglia, F. *et al.* Tracking morphological changes and slope instability using spaceborne and ground-based SAR data. *Geomorphology* **300**, 95–112 (2018).

22. Voight, B. & Elsworth, D. Failure of volcano slopes. *Géotechnique* **47**, 1–31 (1997).

23. Watts, A. B. & Masson, D. G. A giant landslide on the north flank of Tenerife, Canary Islands. *J. Geophys. Res. Solid Earth* **100**, 24487–24498 (1995).

24. Carracedo, J. C. Growth, structure, instability and collapse of Canarian volcanoes and comparisons with Hawaiian volcanoes. *J. Volcanol. Geotherm. Res.* **94**, 1–19 (1999).

25. Carracedo, J. C., Day, S. J., Guillou, H. & Pérez Torrado, F. J. Giant Quaternary landslides in the evolution of La Palma and El Hierro, Canary Islands. *J. Volcanol. Geotherm. Res.* **94**, 169–190 (1999).

Supplementary information: Figures S1-2, Table S1 and Movies S1-3 are included as supplementary information.

Acknowledgments: Earthquake locations and moment tensor solutions were obtained from the GEOFON programme of the GFZ German Research Centre for Geosciences using data from the GEVN partner networks. The authors thank Profs David Bond and Dan Parsons for comments on an early draft of this manuscript.

Funding: N/A

Author information

Contributions: RW conceptualized the project, contributed to the formal analysis, investigation, methodology, validation and visualisation and is responsible for the project administration and data curation. PR lead the formal analysis, investigation, methodology, validation and visualization. MG contributed to the formal analysis, investigation, validation and is responsible for the SAR processing. All authors discussed the results and contributed to the writing of the manuscript.

Conflict of interest: Authors declare no competing interests.

Corresponding Author: Correspondence to Rebecca Williams

Supplementary information for

Small flank failure of Anak Krakatau Volcano caused catastrophic December 2018 Indonesian tsunami

Authors: Rebecca Williams[1]*, Pete Rowley[1], Matthew C. Garthwaite[2]
Affiliations: [1]Department of Geography, Geology & Environment, University of Hull, Hull, UK.
[2]Positioning and Community Safety Division, Geoscience Australia, Canberra, ACT, Australia.
*Correspondence to: Rebecca.williams@hull.ac.uk.

This supplementary information includes:

Figs. S1 to S2
Tables S1
Captions for Movies S1 to S3

Other Supplementary Information for this manuscript include the following:

Movies S1 to S3

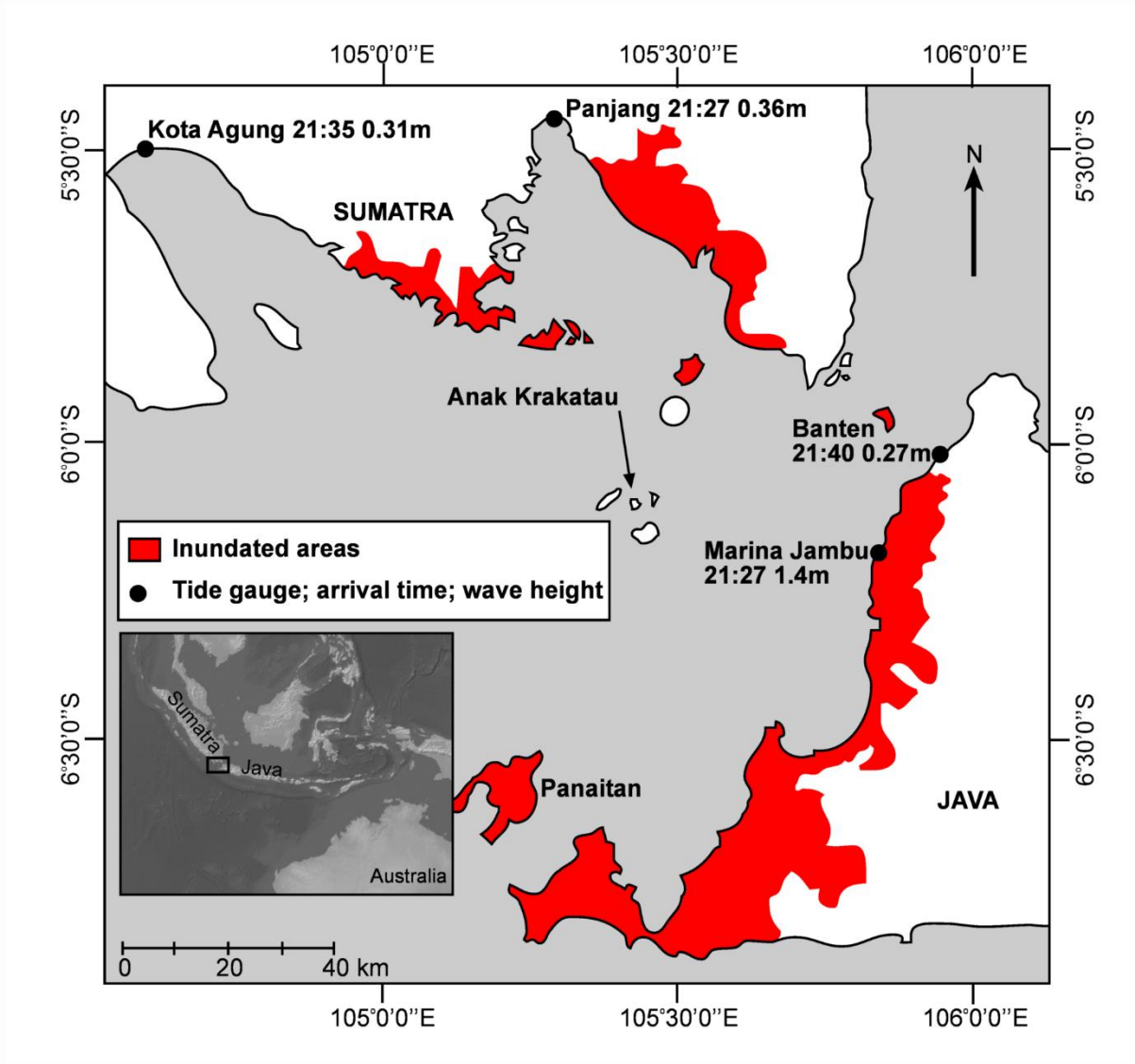

Fig. S1.

Location map of Anak Krakatau showing tide gauges in the Sunda Strait with wave arrival times and wave heights of the 22 December 2018 tsunami. Red zones show coastal areas inundated by the tsunami, adapted from Tsunami selat sunda provinsi Banten dan Lampung map created by Badan Nasional Penanggulangan Bencana dated 28 December 2018[2]. Wave heights and arrival times given by Pusat Vulkanologi dan Mitigasi Bencana Geologi in a press release dated 24 December 2018[6].

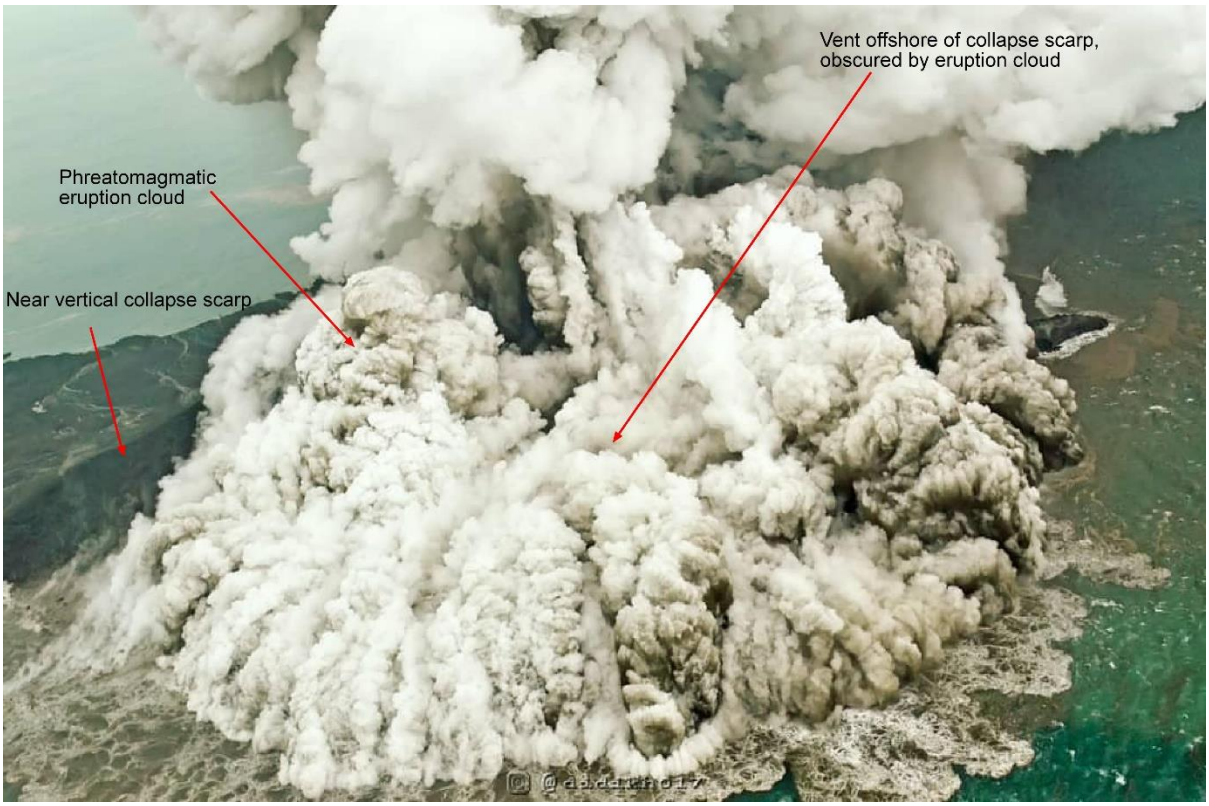

Fig. S2.

Image of the phreatomagmatic eruption taken on the 23 December 17:06 WIB. The steep scarp (near vertical) created by the flank failure can be seen behind the eruption plume. Photo direction towards ESE. Image credit, used with permission: Instagram @didikh017

Table S1.

Details of the Sentinel-1 SAR images used in this study. Elevation and Azimuth angles are for a looking vector towards the satellite originating at the summit cone of Anak Krakatau prior to the flank failure and tsunami. Italicised entries denote images captured before the 22 December 2018 event occurred.

Relative orbit	Pass	Satellite	Acquisition Date (UTC)	Time (UTC)	Days since previous	Elevation (deg)	Azimuth (deg)
171	*Ascending*	*S1A*	*7/12/2018*	*11:23:07*	-	*46.9*	*257.5*
171	*Ascending*	*S1A*	*19/12/2018*	*11:23:06*	*12*	*46.9*	*257.5*
171	Ascending	S1B	25/12/2018	11:22:35	6	46.9	257.5
171	Ascending	S1A	31/12/2018	11:23:06	6	46.9	257.5
171	Ascending	S1A	12/1/2019	11:23:05	12	46.9	257.5
47	*Descending*	*S1A*	*28/11/2018*	*22:33:45*	-	*45.1*	*102.6*
47	*Descending*	*S1A*	*10/12/2018*	*22:33:45*	*12*	*45.1*	*102.6*
47	Descending	S1A	22/12/2018	22:33:44	12	45.1	102.6
47	Descending	S1B	28/12/2018	22:33:06	6	45.1	102.6
47	Descending	S1A	3/1/2019	22:33:44	6	45.1	102.6
47	Descending	S1A	15/1/2019	22:33:44	12	45.1	102.6
120	*Descending*	*S1A*	*3/12/2018*	*22:41:39*	-	*58.6*	*102.3*
120	*Descending*	*S1A*	*15/12/2018*	*22:41:39*	*12*	*58.6*	*102.3*
120	Descending	S1A	27/12/2018	22:41:38	12	58.6	102.3
120	Descending	S1B	2/1/2019	22:41:04	6	58.6	102.3
120	Descending	S1A	8/1/2019	22:41:38	6	58.6	102.3
120	Descending	S1A	20/1/2019	22:41:38	12	58.6	102.3

Movie S1.

Animated compilation of Sentinel-1 SAR backscatter images in the native radar viewing geometry (T120D). Annotated labels give the viewing geometry (relative orbit and pass direction) and the image capture date (UTC). Image x-axis is the range direction and y-axis is the azimuth, or along-track direction of the radar viewing geometry. Details of the three viewing geometries are given in Table S1.

Movie S2.

Animated compilation of Sentinel-1 SAR backscatter images in the native radar viewing geometry (T171A). Annotated labels give the viewing geometry (relative orbit and pass direction) and the image capture date (UTC). Image x-axis is the range direction and y-axis is the azimuth, or along-track direction of the radar viewing geometry. Details of the three viewing geometries are given in Table S1.

Movie S3.

Animated compilation of Sentinel-1 SAR backscatter images in the native radar viewing geometry (T047D). Annotated labels give the viewing geometry (relative orbit and pass direction) and the image capture date (UTC). Image x-axis is the range direction and y-axis is the azimuth, or along-track direction of the radar viewing geometry. Details of the three viewing geometries are given in Table S1.